

Acoustic Tomography at Basin Scales and Clock Errors

Anisim A. Silivra, John L. Spiesberger, Anatoly L. Fabrikant, and Harley E. Hurlburt

Abstract— A basin-scale acoustic tomography simulation is carried out for the northeast Pacific ocean to determine the accuracy with which time must be kept at the sources when clocks at the receivers are accurate. A sequential Kalman filter is used to estimate sound-speed fluctuations and clock errors. Sound-speed fluctuations in the simulated ocean are estimated from an eddy-resolving hydrodynamic model of the Pacific forced by realistic wind fields at daily resolution from 1981–1993. The model output resembles features associated with El Niño and the Southern Oscillation, as well as many other features of the ocean’s circulation. Using a Rossby-wave resolving acoustic array of four fixed sources and twenty drifting receivers, we find that the percentage of the modeled ocean’s sound-speed variance accounted for with tomography is 92% at 400-km resolution, regardless of the accuracy of the clocks. Clocks which drift up to hundreds of seconds of error or more for a year do not degrade tomographic images of the model ocean. Tomographic reconstructions of the sound-speed field are insensitive to clock error primarily because of the wide variety of distances between the receivers from each source. Every receiver “sees” the same clock error from each source, regardless of section length, but the sound-speed fluctuations in the modeled ocean cannot yield travel times which lead to systematic changes in travel time that are independent of section length. The Kalman filter is thus able to map the sound-speed field accurately in the presence of large errors at the source’s clocks.

Index Terms—Acoustic tomography, clocks, Kalman filtering.

I. INTRODUCTION

MUNK and Wunsch [1] suggested using the delays of acoustic pulses between sources and receivers to reconstruct the sound-speed field in the ocean using tomographic techniques. To do this, they stated that time must be maintained to the order of 10 ms. Later, Munk *et al.* [2, p. 173] state that “travel times need to be measured with a precision of a few milliseconds, corresponding to a few parts per million over 1 Mm range.” To the best of our knowledge, there has been no subsequent quantitative examination of this criterion. Since clock errors at the acoustic source directly affect the

arrival time at receivers, it seems obvious that large clock errors can corrupt travel-time data to the extent of not being able to accurately map the sound-speed field with tomography. A one millisecond clock error is easy to maintain if the time base for the clock is maintained via a facility on shore or is in communication with satellites. However, when acoustic sources are placed on autonomous subsurface moorings, one relies on an onboard frequency standard to compute an accurate time. To maintain a millisecond accuracy over the period of a year requires a clock with a fractional frequency error of about 10^{-11} or better. This clock accuracy is not easy to achieve from an engineering point of view [2, p. 208]. With a two-oscillator scheme, a low-power but inaccurate frequency standard keeps time with its frequency error measured several times per day by turning on an accurate but power-hungry Rubidium frequency standard [3]. When a 10-W Rubidium is powered for fifteen minutes four times a day during a year, the required energy is about 3×10^7 J. This is comparable to a standard alkaline battery pack containing 7×10^7 J, the energy typically used for tomographic transmissions during a year. The additional batteries required to maintain an accurate time are expensive and add significantly to the weight of the instruments to be moored. Paradoxically, simulations in this paper show that the acoustic source’s clock may have errors of hundreds of seconds or more and not affect the accuracy of tomographic maps of the ocean’s large-scale structure. Ocean acoustic tomography is not the only application which uses independent clocks to measure the time delay between the moments of pulse radiation and reception [4].

Clock errors occur due to a deviation of the frequency standard used for timekeeping. Consequently, the process of producing clock error may take on a deterministic rather than random character. As a result, the clock error is a sum of a relatively large systematic bias, which can slowly change with time, and a relatively small random component [5, Fig. 6]. We take this into account when we later formulate an approach for modeling clock errors.

For underwater acoustic tomography, it is natural to include clock errors as additional parameters to the set of parameters to be estimated [6], [2]. In this case, clock errors are to be estimated with a certain accuracy and are effectively subtracted from the data so that the estimation of other model parameters could be done using more realistic values from the data set.

II. DESCRIPTION OF A MODEL

A. Ocean Model

The region for the tomographic simulation has a southwest coordinate at 20.5° N, 192.5° W and north-east coordinate

Manuscript received April 3, 1996; revised November 5, 1996. This work was supported by the Strategic Environmental Research and Development Program (SERDP), managed by the Advanced Research Projects Agency Grant MDA972-931-0004, and by the Office of Naval Research Grant N00014-95-1-0755.

A. A. Silivra is with the Applied Research Laboratory, Pennsylvania State University, State College, PA 16804 USA.

J. L. Spiesberger is with the Applied Research Laboratory and the Department of Meteorology, Pennsylvania State University, University Park, PA 16802 USA.

A. L. Fabrikant is with the Department of Meteorology, Pennsylvania State University, University Park, PA 16802 USA.

H. E. Hurlburt is with the Naval Research Laboratory, Stennis Space Center, Bay St. Louis, MS 39522 USA.

Publisher Item Identifier S 0364-9059(97)01422-2.

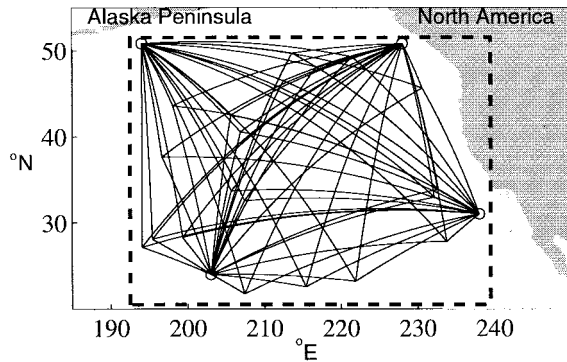


Fig. 1. Region of the tomography simulations in the northeast Pacific. Circles mark the positions of sources. Geodesic lines connect sources and drifting receivers. The locations of drifting receivers are shown for day 110 of the model year 1985.

at 51.5° N, 239.5° W (Fig. 1). This is a subdomain of the ocean model described later in this section. The tomographic instruments include four fixed acoustic sources and twenty drifting receivers with navigational accuracy of 10 m. The location of drifting receivers for all moments of time for the year of 1985, as well as sound-speed perturbations in the ocean, are computed with the eddy-resolving hydrodynamic Naval Research Laboratories (NRL) layered ocean model [7]. This model represents in a quasi-realistic way some of the ocean variations due to El Niño and the Southern Oscillation, which are a major part of the Pacific Ocean large-scale variability. The model was used to successfully interpret many features of multiscale ocean circulation including a Rossby wave generated by the 1982–1983 El Niño [7], [8]. Modeled travel times are overwhelmingly due to first-mode baroclinic Rossby waves linked to El Niño and the Southern Oscillation [9]. The effects of eddies, currents, and other modeled features contribute less than a percent of the total modeled variance in travel time [9].

The NRL model includes six layers of constant density, realistic bottom topography, and a horizontal grid resolution of $\frac{1}{8}^\circ$. Between 1981–1993, the model is forced by daily wind products from the European Center for Medium Range Weather Forecast (ECMWF) between 20° S and 62° N in the Pacific. See [9], [10] for detailed descriptions of this model.

In this paper, sound speed is computed as described in [9]. Sound-speed perturbations are computed by assuming that vertical displacements in the model's layers lead to adiabatic changes in the speed of sound.

The sound-speed perturbations in the model reach maximum values in the main thermocline where the vertical profile of the sound-speed is not-adiabatic due to heating from the surface [11, Fig. 3]. Typical sound-speed variations are about 4 m/s at 300 m depth. Below the main thermocline the sound-speed profile is nearly adiabatic and vertical particle displacements have little effect on sound speed.

B. Synthesis of Acoustic Travel Times

The data, d , for the forward problem are the travel times, T , through the simulated sound-speed field minus travel times, T_0 ,

through the reference sound-speed field. The reference sound-speed field is constructed by computing sound-speeds with Del Grosso's algorithm [12] using temperature and salinity versus depth from Levitus's climatological database [13]. The simulated sound-speed field is obtained by adding sound-speed perturbations from the NRL model to the reference field. Each datum, d , is corrupted by adding a clock error, ξ , and pseudorandom noise νr , where ν is the standard deviation of noise related to this measurement, and r is the pseudorandom number with standard deviation 1. Thus, we have

$$d = T - T_0 + \xi + \nu r. \quad (1)$$

The noise variance ν^2 has four contributions. They are:

- 1) precision of measuring the arrival time of a pulse due to the signal-to-noise ratio and the bandwidth of the pulse;
- 2) imperfect corrections to the travel time biases due to eddies;
- 3) imperfect corrections to the travel time biases due to internal waves;
- 4) unmodeled variations at small scales in the NRL ocean model.

At distances of thousands of kilometers, these produce errors of the order 10 ms. A complete description of the simulated noise is given by [11, Eq. (11)].

We do not solve the three-dimensional (3-D) forward problem, but replace it with a computationally more efficient two-dimensional (2-D) sound propagation problem on a horizontal plane. This approximation is excellent and is based on our finding that modeled acoustic travel times are dominated by first-baroclinic-mode Rossby waves [9], [11].

III. KALMAN FILTER

The Global Acoustic Mapping of Ocean Temperature (GAMOT) program [14] has developed a procedure for sequentially assimilating acoustic tomography data [11]. A sequential Kalman filter [15], [16] is used to estimate the sound-speed field in the model, errors in the positions of the acoustic sources and receivers, and errors in the timekeeping at the acoustic sources. Reference [11] gives a detailed description of this Kalman filter, except for the handling of clock-error parameters. Handling of the clock-error parameter will be discussed later in this section. This filter has been previously used to demonstrate that modeled Rossby waves can be well resolved in the northeast Pacific using sources and receivers whose measured positions have errors of a kilometer [11].

A. Summary of the Kalman Filter Implementation

The Kalman filter gives us a least-square estimation of model parameters on the basis of simulated data and *a priori* information on the scales of the modeled parameters. The modeled 2-D sound-speed field is represented by a 2-D Fourier decomposition which provides approximately 100-km resolution. A total of 1457 harmonics are required to obtain this resolution. We include clock errors and source/receiver position errors in the vector of model parameters, \mathbf{m} . Thus,

the model consists of 1457 amplitudes of Fourier harmonics, 72 parameters accounting for source/receiver position errors, and four parameters for clock errors, one for each source, for a total of 1533 parameters.

Using a linear approach, we assume that data, \mathbf{d} , and model parameters, \mathbf{m} , satisfy a relation

$$\mathbf{d} = \hat{\mathbf{G}}\mathbf{m} + \mathbf{n} \quad (2)$$

where $\hat{\mathbf{G}}$ is a matrix of model parameter's weights, \mathbf{n} is a vector of noise with zero mean and variance ν^2 . The least-square estimation of the model parameters is given by

$$\mathbf{m}^+ = \mathbf{m}^- + \hat{\mathbf{K}}(\mathbf{d} - \hat{\mathbf{G}}\mathbf{m}^-) \quad (3)$$

where \mathbf{m}^+ , \mathbf{m}^- are updated and previous value of model parameters, so that $\mathbf{d} - \hat{\mathbf{G}}\mathbf{m}^-$ is an innovation vector. The Kalman gain matrix is

$$\hat{\mathbf{K}} = \hat{\mathbf{M}}^- \hat{\mathbf{G}}^T (\hat{\mathbf{G}}\hat{\mathbf{M}}^- \hat{\mathbf{G}}^T + \nu^2 \hat{\mathbf{I}})^{-1}$$

where $\hat{\mathbf{M}}^-$ is a positive definite square matrix of model parameter covariances just prior to data assimilation. The identity matrix is $\hat{\mathbf{I}}$. The error covariance matrix just after data assimilation is

$$\hat{\mathbf{M}}^+ = (\hat{\mathbf{I}} - \hat{\mathbf{K}}\hat{\mathbf{G}})\hat{\mathbf{M}}^-. \quad (4)$$

Data are simulated using an acoustic propagation model and subsequently assimilated at about 15-day intervals. Thus, we estimate the state of the ocean at the particular moment of time allowing for the previous estimation of model parameters and their covariances. It should be noted that the previous time-step estimation is transitioned before combining with the current data. For the ocean model parameters, we use modified persistence transitioning [18] which provides for exponential decay of ocean model parameters and corresponding covariances toward their *a priori* values. Time constants for all ocean harmonics are calculated from the NRL ocean model. Typical values of the time constants are within the limits of 400 days for the long-wave perturbations to 30 days for the short-wave perturbations.

The sequential Kalman filter is run in the forward and backward time directions. Estimates of model parameters and their errors are obtained by optimally combining the results of the forward and backward runs as described elsewhere [11].

B. Model Parameters for Clock Errors

For basin scale tomography, we can use either a “good” clock, which is characterized by a fractional frequency error of $\delta \equiv \frac{\Delta f}{f} \leq 10^{-11}$, or a “bad” clock with $\delta = 10^{-8}$ or more. This means that “good” clocks may deviate from geophysical time about 0.0003 s per year, while “bad” clocks may deviate by as much as 0.3 s per year. Hereafter, it is assumed that the maximum growth rate of clock error, δ , is known. The initial offset of a clock which might occur after deployment could be also assumed to be known, for example, from a measurement from a nearby ship [17]. Further, we assume that the standard deviation of the initial clock offset is $\sigma_\xi(0)$.

The clock error for each clock was simulated as a polynomial expression

$$\xi = a_0 + a_1 t + a_2 t^2 + a_3 r \quad (5)$$

where a_i are constants, t is time elapsed after deployment, and r is a random number with a standard deviation of unity.

The coefficients a_i in (5) are chosen so that at $t = 0$ the clock error does not exceed the initial value $\sigma_\xi(0)$ (in our case $\sigma_\xi(0) = 1$ ms), corresponding to the offset of clocks after the deployment, and further remained within the interval $|\xi - \sigma_\xi(0)| \leq \delta \cdot t$. At the same time, the growth rate of clock error must not exceed $|\frac{d\xi}{dt}| \leq \delta$, where δ is the fractional frequency error of the clock. The coefficient a_3 , describing the random part of the clock error, is chosen to be much smaller than a_0 . And, since the simulated clock error for $t = 0$ must be consistent with the *a priori* standard deviation of the clock error $\sigma_\xi(0)$, the coefficients $a_{0,3}$ satisfy the relation

$$a_0^2 + a_3^2 = \sigma_\xi^2(0). \quad (6)$$

Simulated clock errors are shown in Fig. 2.

Let m_ξ be a model parameter which corresponds to the clock error. We need to specify how to handle this parameter and its covariance between time steps. We assume that it is appropriate to estimate the clock error between time steps as

$$m_\xi(t + \Delta t) = m_\xi(t) \quad (7)$$

i.e., the modeled error at time t is the same as at time $t + \Delta t$, where Δt is the duration of the time step.

Since a clock error cannot change more than $(\delta \cdot \Delta t)$ between time steps, the transition rule (7) means that possible inaccuracy of transitioning does not exceed $(\delta \cdot \Delta t)$. This value could be used as an estimate of noise introduced by the transition rule (7). But, taking into account a deterministic character of this inaccuracy, we prefer to choose the transition for the variance of a clock error in the form

$$\sigma_\xi^2(t + \Delta t) = (\sigma_\xi(t) + \delta \cdot \Delta t)^2 \quad (8)$$

where $\sigma_\xi(t)$ is the estimate of the standard deviation of the clock error at the time moment t , δ is *a priori* known growth rate for the clock error. It should be noted that in this way we overestimate the variance of the clock error rather than underestimate it.

IV. TOMOGRAPHY SIMULATIONS

In all cases in this paper, the model fits the simulated data within two standard deviations. This means that the model is consistent with the simulated data.

Curves 1–4 in Fig. 2 show simulations of clock errors produced by “bad” clocks with fractional frequency errors of $\delta = 10^{-8}$. Similar errors are observed in clocks used in tomography experiments [5]. Modeled sound-speed fluctuations for a section yield travel-time changes of about 0.1 s (curve 5, Fig. 2). Travel times come in sooner than predicted for the reference ocean, indicating the average speed of sound is faster than the reference along this section. When clock errors are added, the arrival times of sound come in later than given by the reference travel times (curve 6, Fig. 2). Without modeling

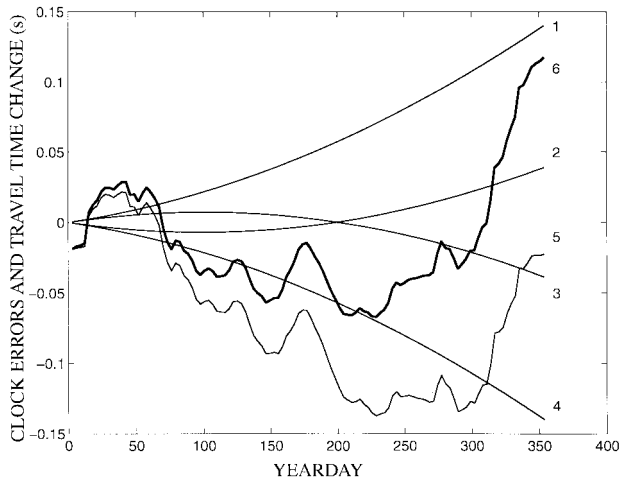


Fig. 2. Simulated clock errors at sources 1–4 having a fractional frequency error of 10^{-8} during a model year. The simulated acoustic travel-time changes for a 2500-km section are shown without clock error (curve 5) and with clock error (curve 6).

clock errors, one might incorrectly conclude the average speed of sound is slower than the reference speeds along the section. It would seem that tomographic reconstructions with such corrupted data would yield a very inaccurate tomography result. Nevertheless, the sequential estimation implemented by the Kalman filter is able to account for the clock error and effectively correct the data.

The assimilation of the data for each time step results in the decrease of variances of all parameters including clock-error variances, while between time steps they are allowed to grow due to the transition rules specified above. Eventually, we achieve a dynamically steady state for which an increase of clock-error variances between time steps is compensated by a decrease of clock-error variances due to assimilation of data.

In Fig. 3, we see that a dynamically steady state is achieved with regard to the clock errors in a few months. The standard deviation of a clock-error estimation is approximately $\sigma_\xi \simeq 0.03$ s for the major part of the year for which the tomography is done. The estimates of clock errors themselves are shown in Fig. 4. In comparison, the clocks themselves are about 0.3 s off at year-end.

We find that large-scale tomographic reconstructions of the sound-speed field are insensitive to the clock errors at the sources (Fig. 5). The tomographic reconstructions are made for clocks having fractional frequency errors of $\delta = 10^{-11}$, 10^{-8} , and 10^{-5} . These errors lead to clock offsets of about 0.0003, 0.3, and 300 s, respectively, after a year has elapsed.

The quality of a tomographic reconstruction is estimated by dividing the simulation domain in Fig. 5 into 96 squares with sides 4° latitude by 4° longitude. From these, a subset of 54 squares is chosen. The subset excludes squares on the perimeter and on the second from the most right-hand column of the simulation domain so as to avoid areas containing few tomographic sections. In each square of the subdomain, the tomographically estimated sound-speed field is spatially averaged. The variance of this average at some particular time step for the n th square is denoted by $\sigma_{\text{TOMO}}^2(n)$. This

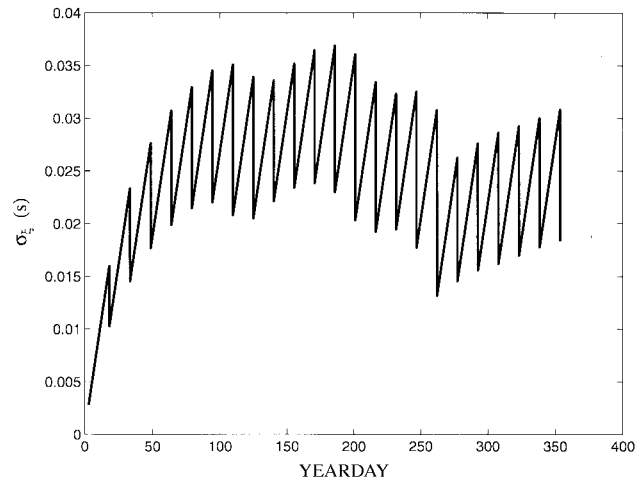


Fig. 3. The Kalman filter's estimate of the standard deviation of clock error as a function of the day throughout a model year. Errors decrease following data assimilation at about 15-day intervals and then grow until the next data are assimilated. This leads to the characteristic sawtooth pattern of parameter errors associated with sequential Kalman filters.

is compared to the *a priori* variance of the sound-speed field at 300-m depth denoted by $\sigma_{\text{NRL}}^2(n)$. This variance is obtained from the *a priori* covariances used by the Kalman filter [11, Section IV]. The percentage of sound-speed variance accounted for with the data in square n is

$$F(n) = 100 \left(1 - \frac{\sigma_{\text{TOMO}}^2(n)}{\sigma_{\text{NRL}}^2(n)} \right). \quad (9)$$

If $F(n)$ equals 95%, then tomographic reconstructions account for 95% of the variance of the sound-speed field in the n th square. The average value of $F(n)$ in the subdomain is

$$\bar{F} \equiv \frac{1}{54} \sum_{n=1}^{54} F(n). \quad (10)$$

The value of \bar{F} is 91.2%, 90.9%, and 90.7% for clocks having fractional frequency errors of $\delta = 10^{-11}$, 10^{-8} , and 10^{-5} , respectively. Thus, the quality of the tomographic reconstruction is insensitive to the error of the clock used to set the transmission time of the acoustic signal.

V. INTERPRETATION

The paradox that the simulated sound-speed field can be mapped well despite huge errors in the source's clocks requires an explanation. Suppose the sound-speed field is simplified so as to have only a fundamental harmonic, so there is only one parameter to estimate for the sound-speed field. That parameter gives the speed of sound everywhere in space.

Consider case 1, where two receivers are about equidistant from a source (Fig. 6). If there is an error in the source's clock, both receivers register the same offset due to this error. The actual sound-speed field would also affect the arrival times at the two receivers in identical ways. Since the clock errors and the corrections to the constant reference sound-speed field yield the same kind of arrival time changes at both receivers, it is difficult in this case to estimate the sound-speed field accurately.

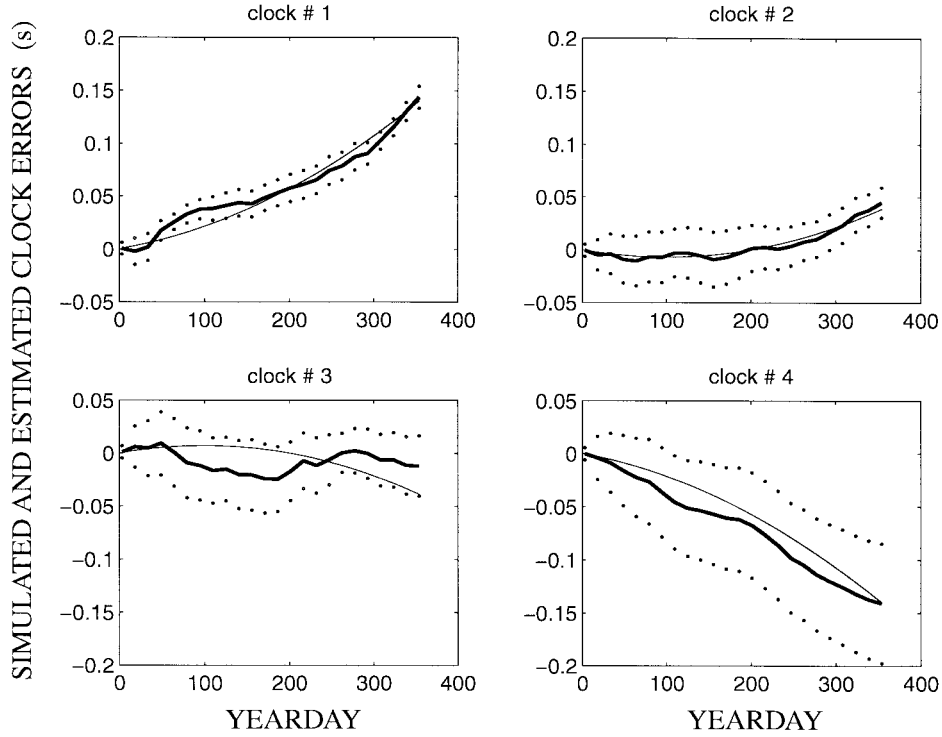


Fig. 4. Simulated clock errors with fractional frequency errors of 10^{-8} for four sources (light solid line) compared with the Kalman filter's estimates of clock errors (dark solid lines) and the errors of the clock errors (dotted lines). Errors indicate two standard deviations. The simulated clock errors are the same as shown in Fig. 2.

In case 2, one receiver is much closer to the source than the other. The error in the clock affects the arrival times at both receivers by the same amount. However, the unknown constant sound-speed perturbation affects the arrival times at the two receivers differently. If the constant sound-speed perturbation is δc , then the travel-time changes at receivers one and two are $-\delta c L_1 / c_0^2$ and $-\delta c L_2 / c_0^2$, respectively. Here, the reference speed of sound is c_0 . These perturbations are different because L_1 is quite different than L_2 . In this case, we expect to be able to untangle the clock error from the sound-speed perturbation of interest. When cases 1 and 2 are modeled analytically, these conclusions are verified (see the Appendix).

Case 2 is very much like the simulations shown in this paper. The receivers have quite different distances from the source. The arrival times from the source are the same due to clock errors, but are different due to sound-speed fluctuations. Since only the large-scale perturbations in the modeled ocean affect travel-time changes significantly [11], [9], our model ocean is somewhat like the simplified case considered above, i.e., only the fundamental harmonic affects the acoustic travel times.

APPENDIX

TOMOGRAPHY AND RECEIVER SECTION LENGTH

Assume that the model consists of two parameters: the fundamental harmonic for the sound-speed perturbation, m_1 , and the clock error, m_2 . The *a priori* standard deviations of these parameters are σ_1 and σ_2 , respectively. The distances between the source and the two receivers are L_1 and L_2

respectively, and the reference speed of sound is c_0 . The data are related to the model using (2) where

$$\hat{\mathbf{G}} = \begin{pmatrix} -\frac{L_1}{c_0^2} & 1 \\ -\frac{L_2}{c_0^2} & 1 \end{pmatrix}$$

and

$$\mathbf{n} = \begin{pmatrix} \nu_1 \\ \nu_2 \end{pmatrix}.$$

The data from receivers one and two are then

$$\begin{aligned} d_1 &= -\frac{L_1}{c_0^2} \bar{m}_1 + \bar{m}_2 + \nu_1 \\ d_2 &= -\frac{L_2}{c_0^2} \bar{m}_1 + \bar{m}_2 + \nu_2 \end{aligned}$$

where \bar{m}_1 and \bar{m}_2 denote the true values for the sound-speed perturbation and clock error, respectively. We now assume that the effects of the sound-speed perturbation and the clock error contribute to the travel-time data at each receiver such that the geometric mean of the effects of the sound-speed perturbation on travel times equals the effects of the clock error on the travel times. Thus

$$\frac{\sqrt{L_1 L_2}}{c_0^2} \sigma_1 = \sigma_2.$$

In all cases below, we assume a high signal-to-noise ratio. We use (3) to estimate the model parameter vector \mathbf{m}^+ with $\mathbf{m}^- = \mathbf{0}$. We also use (4) to estimate the model-covariance

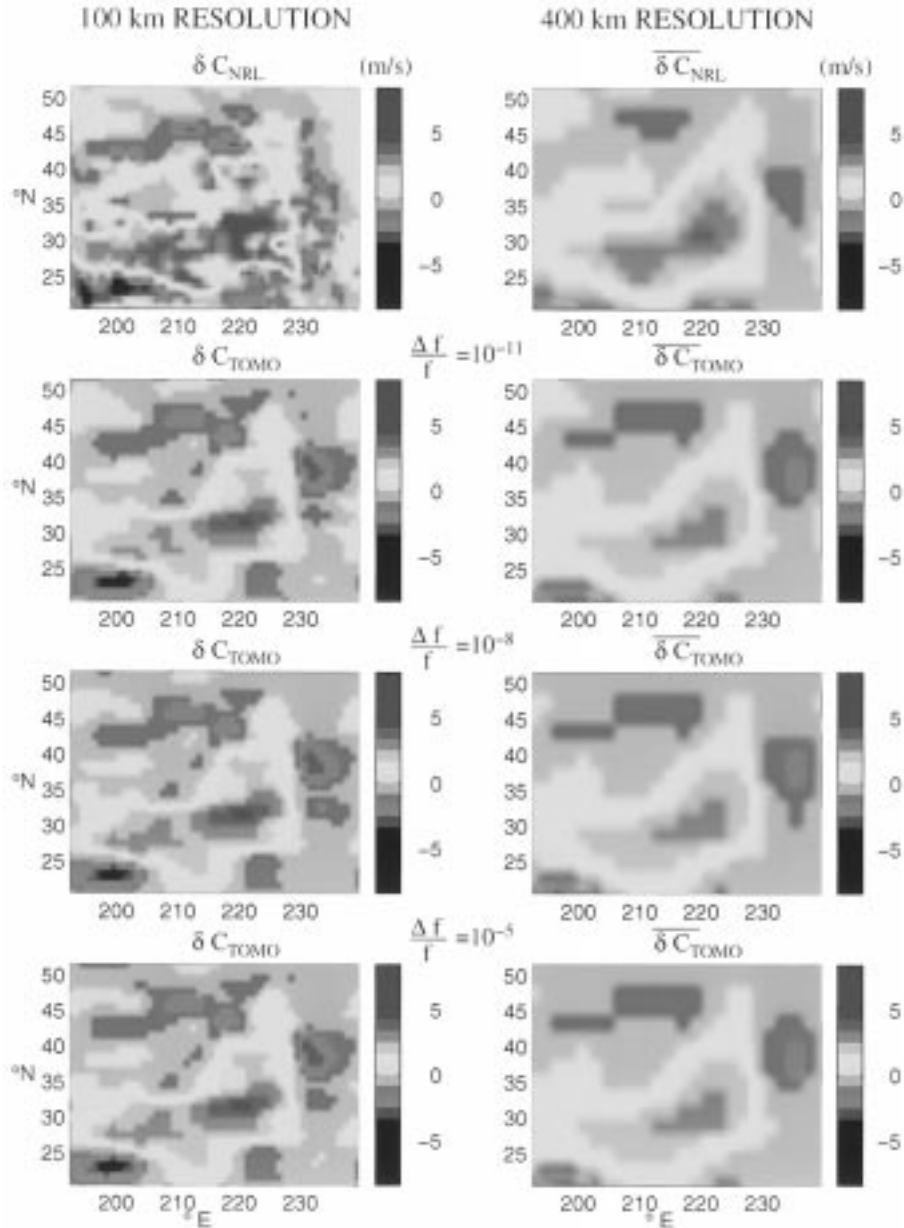


Fig. 5. The top panels indicate sound-speed perturbations from the NRL model at 100- and 400-km resolution in the dashed model domain shown in Fig. 1. The bright red region is the modeled Rossby wave in 1985. The three lower rows show tomographic reconstructions of the sound-speed field for four sources and twenty drifting receivers on day 110 in 1985, for the indicated fractional frequency errors of clocks at the acoustic sources. After a year, fractional frequency errors of 10^{-11} , 10^{-8} , and 10^{-5} , lead to clock errors of about 0.0003, 0.3, and 300 s, respectively. The tomographic reconstructions are insensitive to clock errors.

matrix, $\hat{\mathbf{M}}^+$, following assimilation of data. The *a priori* error-covariance matrix is

$$\hat{\mathbf{M}}^- = \begin{pmatrix} \sigma_1^2 & 0 \\ 0 & \sigma_2^2 \end{pmatrix}.$$

Case 1: The distances from the source to each receiver are equal in this case, so $L_1 = L_2$. After computing the Kalman gain matrix, the model parameters have the solution

$$m_1^+ \cong \frac{\bar{m}_1}{2} - \frac{c_0^2}{2L_1} \bar{m}_2 \quad (\text{A1})$$

$$m_2^+ \cong -\frac{L_1}{2c_0^2} \bar{m}_1 + \frac{1}{2} \bar{m}_2. \quad (\text{A2})$$

The error-covariance matrix for these model parameters is

$$\hat{\mathbf{M}}^+ \cong \frac{1}{2} \begin{pmatrix} \sigma_1^2 & \sigma_1 \sigma_2 \\ \sigma_1 \sigma_2 & \sigma_2^2 \end{pmatrix}$$

with variances of model parameters being half of their initial values. In this case, errors in the clock significantly degrade the accuracy with which the sound-speed and clock-error parameters are estimated.

Case 2: In this case, receiver 1 is much closer to the source than receiver 2, so we have $L_1 \ll L_2$. The model parameters have the solution

$$m_1^+ \cong \bar{m}_1 \quad (\text{A3})$$

$$m_2^+ \cong \bar{m}_2. \quad (\text{A4})$$

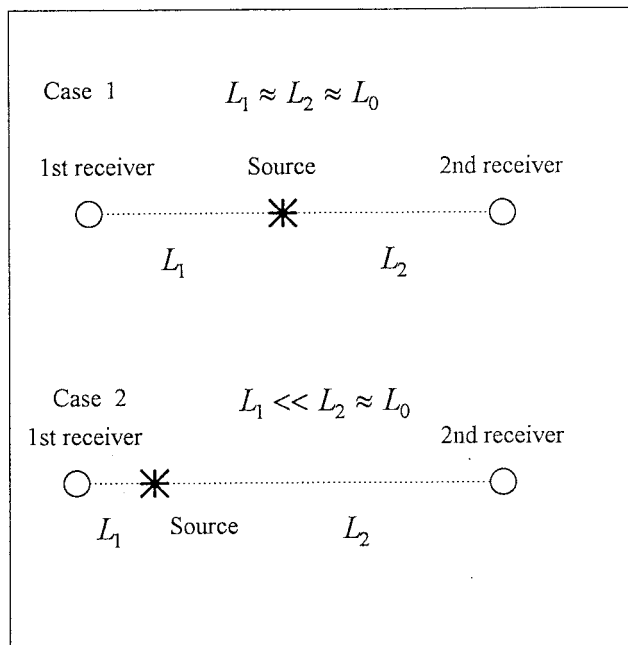


Fig. 6. In case 1, two receivers are about the same distance from an acoustic source. In case 2, two receivers have greatly different distances from the acoustic source.

The error-covariance matrix for these model parameters is

$$\hat{\mathbf{M}}^+ \approx \frac{L_1}{L_2} \begin{pmatrix} 2\sigma_1^2 & 0 \\ 0 & 2\sigma_2^2 \end{pmatrix}.$$

Since $L_1 \ll L_2$, the covariances of the updated model parameters are much less than their *a priori* values. The Kalman filter obtains accurate answers for both the sound-speed perturbation and the correction to the clock.

ACKNOWLEDGMENT

The authors thank M. Keller and B. Wong for assistance with the computations and figures.

REFERENCES

- [1] W. Munk and C. Wunsch, "Ocean acoustic tomography: A scheme for large scale monitoring," *Deep-Sea Res.*, vol. 26, pp. 123–161, 1979.
- [2] W. Munk, P. Worcester, and C. Wunsch, *Ocean Acoustic Tomography*. Cambridge: Cambridge Univ. Press, 1995.
- [3] P. F. Worcester, D. A. Peckham, K. R. Hardy, and F. O. Dormer, "AVATAR: Second-generation transceiver electronics for ocean acoustic tomography," in *Oceans 85: Ocean Engineering and the Environment*, San Diego, CA, 12–14 Nov. 1985, pp. 654–662.
- [4] Y. C. Lee, "RAIM availability for GPS augmented with barometric altimeter aiding and clock coasting," *Navigation, J. Inst. Navig.*, vol. 40, pp. 179–198, 1993.
- [5] J. L. Spiesberger and J. B. Bowlin, "A telemetry scheme for ocean acoustic tomography: Real time monitoring," *J. Marine Env. Eng.*, vol. 1, pp. 1–22, 1993.
- [6] B. Cornuelle, "Simulations of acoustic tomography array performance with untracked or drifting sources and receivers," *J. Geophys. Res.*, vol. 90, no. C5, pp. 9079–9088, 1985.
- [7] H. E. Hurlburt, A. J. Wallcraft, Z. Sirkes, and E. J. Metzger, "Modeling of the global and Pacific oceans: On the path to eddy-resolving ocean predictions," *Oceanography*, vol. 5, pp. 9–18, 1992.
- [8] G. A. Jacobs, H. E. Hurlburt, J. C. Kindle, E. J. Metzger, J. L. Mitchell, and W. J. Teague, "Decade scale transpacific propagation and warming effects of an El Niño anomaly," *Nature*, vol. 370, pp. 360–363, 1994.

- [9] J. L. Spiesberger, H. E. Hurlburt, M. Johnson, M. Keller, S. Meyers, and J. O'Brien, "Acoustic thermometry data compared with two climate change models of the ocean: The importance of Rossby waves and ENSO in modifying the ocean interior," *Dynamics of Atmospheres and Oceans*, submitted for publication.
- [10] H. E. Hurlburt, A. J. Wallcraft, W. J. Schmitz, Jr., P. J. Hogan, and E. J. Metzger, "Dynamics of the Kuroshio/Oyashio current system using eddy-resolving models of the North Pacific Ocean," *J. Geophys. Res.*, vol. 101, pp. 941–976, 1996.
- [11] J. L. Spiesberger, A. L. Fabrikant, A. A. Silvra, and H. E. Hurlburt, "Mapping climatic temperature changes in the ocean with acoustic tomography: Navigational requirements," this issue, pp. 136–150.
- [12] V. A. Del Grosso, "New equation for the speed of sound in natural waters with comparison to other equations," *J. Acoust. Soc. Amer.*, vol. 56, pp. 1084–1091, 1974.
- [13] S. Levitus, "Climatological atlas of the world ocean," *NOAA Prof. Pap.*, US Government Printing Office, Washington, DC, vol. 13, 1982.
- [14] J. L. Spiesberger, D. E. Frye, J. J. O'Brien, H. Hurlburt, J. McCaffrey, M. Johnson, M. Leach, and J. Kenny, "Global acoustic mapping of ocean temperatures (GAMOT)," in *Proc. Second European Conf. on Underwater Acoustics*, L. Bjorno, Ed. Luxembourg: European Commission, Luxembourg: Office for Official Publications of the European Communities, 1994, vol. II, pp. 1031–1036.
- [15] G. J. Bierman, *Factorization Methods for Discrete Sequential Estimation. Mathematics in Science and Engineering*. New York: Academic, 1977, vol. 128.
- [16] M. Ghil, S. E. Cohn, and A. Dalcher, "Application of sequential estimation to data assimilation, in large-scale oceanographic experiments in the world climate research programme," *WCRP Publ. Ser.*, WMO/ICSU, Geneva, Switzerland, vol. II, no. 1, pp. 341–356, 1983.
- [17] S. P. Liberatore and F. Schuler, "SAIL acoustic modem," in *Internal Report, Woods Hole Oceanographic Institution*. Woods Hole, MA: Ocean Industry Program, 1984.
- [18] B. M. Howe and P. F. Worcester, "Ocean acoustic tomography: Mesoscale velocity," *J. Geophys. Res.*, vol. 92, pp. 3785–3805, 1987.



Anisim A. Silvra was born in Slaviansk, Ukraine, on February 26, 1954. He received the Masters degree in general physics and the Ph.D. degree in theoretical and mathematical physics from Kiev State University in 1976 and 1983, respectively.

In 1983, he began working at Kiev State University on the linear and nonlinear theory of interaction of electromagnetic waves with electron beams and plasmas. In 1994, he joined the Department of Meteorology, Pennsylvania State University (Penn State), University Park, where he contributed to

underwater acoustic tomography simulation and the development of an inverse technique for underdetermined systems. Since 1996, he has been with the Applied Research Laboratory at Penn State.



John L. Spiesberger was born in Jackson, MI, on November 14, 1953. He received the A.B. degree in physics from the University of California at Berkeley in 1975, and the Ph.D. in oceanography from the University of California at San Diego in 1980.

Between 1982–1992, he conducted research at the Woods Hole Oceanographic Institution, Woods Hole, MA, and thereafter joined the Department of Meteorology at the Pennsylvania State University, University Park, with a joint appointment at the Applied Research Laboratory. He has contributed

to the fields of underwater acoustics, physical oceanography, inverse theory, signal processing, and bioacoustics.



Anatoly L. Fabrikant received the M.S. degree in physics and the Ph.D. degree in nonlinear dynamics from the State University of Gorky, Russia, in 1973 and 1980, respectively, and the Ph.D. degree in geophysical fluid dynamics from the Institute of Applied Physics, Russian Academy of Science, Nizhny Novgorod, Russia, in 1991.

He worked for 20 years in the Institute of Applied Physics, Russian Academy of Sciences. After that he worked at Jet Propulsion Laboratory, NASA. Currently, he is a Senior Research Associate in the

Department of Meteorology, Pennsylvania State University, University Park. His research interests are in fluid dynamics, oceanography, wave theory, acoustics, nonlinear dynamics, and remote sensing.

Dr. Fabrikant is a member of the Acoustical Society of America and the American Geophysical Union.



Harley E. Hurlburt received the B.S. degree in physics from Union College, Schenectady, NY, in 1965 and the Ph.D. degree from Florida State University, Tallahassee, in 1974.

Prior to obtaining the Ph.D. degree, he served as a Weather Officer in the USAF (1965–1969). He performed postdoctoral research in the Advanced Studies Program at the National Center for Atmospheric Research in Boulder, CO, from 1974–1975. Since then, he has done ocean modeling for the U.S. Navy, first as a contractor at JAYCOR for the

Naval Research Laboratory in Washington, DC, then in 1977 for the Naval Ocean Research and Development Activity, which later became the Naval Oceanographic and Atmospheric Research Laboratory and which merged with the Naval Research Laboratory in 1992, all in a location at Stennis Space Center, MS. In addition, he is an Adjunct Faculty Member at Florida State University and the University of Southern Mississippi, Hattiesburg. His primary research interests are ocean modeling and prediction, especially the investigation of ocean dynamics using eddy-resolving global and basin-scale ocean models.